Chapter 9

Lessons Learned from Our Recent Research in Chemical Enhanced Oil Recovery (C-EOR) Methods

Bing Wei, Peng Wei, Shuai Zhao and Wanfen Pu

Additional information is available at the end of the chapter

http://dx.doi.org/10.5772/intechopen.71816

Abstract

As a result of the ever-increasing global energy demand coupled with the rapid decline of the oil production, the games of enhanced oil recovery (EOR) are played in many oilfields worldwide especially in China. It was reported that EOR jobs produced 45.1×10^4 m^3/d of oil production rate in 2014 all over the world, proving the significance of these jobs. Due to the complex geology, chemical enhanced oil recovery (C-EOR) methods are considered the predominant technology in China and takes nearly 86% of the total EOR projects currently. This fact motivates us to develop novel and more advanced C-EOR methods for different geological types of Chinese reservoirs such as high temperature and pressure, ultralow permeability, heavy oil reservoirs, etc. Through 20 years' efforts, many advantageous C-EOR methods have been successfully developed in our group and tested in oilfields such as stabilized foam injection, nanofluid flooding, functional polymer flooding, etc. Herein, this chapter summarized the latest experimental results of three representative C-EOR methods. More attentions were given to the relationship between bulk properties and flow behaviors in porous media. The lessons learned from our research in C-EOR were also discussed in this chapter.

Keywords: enhanced oil recovery, chemical flooding, innovative EOR, nanofluid, polymer microsphere, enhanced foam

1. Nanofluid flooding

To date, hydrolyzed polyacrylamide (HPAM) is still the most widely used polymer due to its availability in large quantities with customizable properties (molecular weight, hydrolysis degree, etc.) and low manufacturing cost. However, acrylamide-based polymers are susceptible to chemical, mechanical, thermal, and microbial degradations [1]. In addition, the acrylamide monomers place

detriment to the environment due to its toxicity [2, 3]. Nanofluids, which are obtained through dispersing nanoparticles in the base fluids, are attracting research attentions. The nanofluids usually exhibit high thermal conductivities, which are significant to the development of energy, and have been widely used in drug delivery solar cells, lipase immobilization, soil remediation, lubrication, and hydraulic fracturing of gas and oil. In addition, nanofluids have been introduced to the enhanced oil recovery (EOR) area due to their unique thermal properties and large surface area [4–8]. Many works have been done to study the EOR performance of nanofluids composed of different nanoparticles. Hendraningrat et al. evaluated the displacement efficiency of the nanofluid. They claimed that the nanofluid increased the oil recovery by 7–14.3% and the optimum concentration was 0.05 wt% for water-wet core [9, 10]. The stability of nanofluids was considered as an important factor, which is closely associated with the success of nanofluid flooding [11]. Roustaei et al. demonstrated that the modified silica nanoparticles were able to enhance light oil recovery by reducing interfacial tension and altering wettability [12]. The potential of hydrophobic and lipophilic nanoparticles in EOR was also verified [13–15].

Cellulose is one of the most abundant biopolymers on earth and widely contained in wood, cotton, hemp, and other renewable origins [16–19]. When cellulose is in nanosize, many distinctive properties are therefore created, for example, high strength, chemical accessibility, large surface area, etc., which accordingly cause the increasing attentions in the research community [20, 21].

1.1. Surface grafting

In the interest of further improving the properties of the nanocellulose (NC) toward EOR use, two functional NC samples were successfully prepared in our group *via* surface grafting. The chemical structures and micromorphologies of the three samples are shown in **Figure 1**. **Figure 2** shows the TG/DTG curves of the nanocellulose. It was noted that after surface grafting, the thermal stability of resultant NC (NC-KY and NC-KYSS) was slightly higher than the origin caused by the grafted AMPS and alkyl chains [16, 17, 22, 23].

1.2. Rheological properties of the nanofluids

The shear rate and mass-dependent behavior of nanofluid viscosity are shown in **Figure 3**. All the three nanofluids are pseudoplastic fluids, i.e., shear-thinning fluids. The viscosity of the nanofluid gradually increased with the concentration, which was consistent with the tendency of other relevant polymers as HPAM. After grafting, the viscosity of the nanocellulose was detracted especially NC-KYSS resulted from enlarged molecular space induced by the loaded groups. Nevertheless, a significant thickening power was observed for NC-KYSS at an industrial level as indicated in **Figure 3**. It has been well understood that viscosity of the system is the predominant component in any chemical-based EOR process. Compared with other particle-based nanofluids, the nanocellulose nanofluids are advantageous with noticeable thickening property [17].

1.3. Dispersity of nanocellulose in electrolyte

The colloidal stability of nanofluid is one of the major considerations for EOR. The presence of cations (Na^+, Ca^{2+}, and Mg^{2+}) usually leads the nanocellulose to aggregate and

http://dx.doi.org/10.5772/intechopen.71816

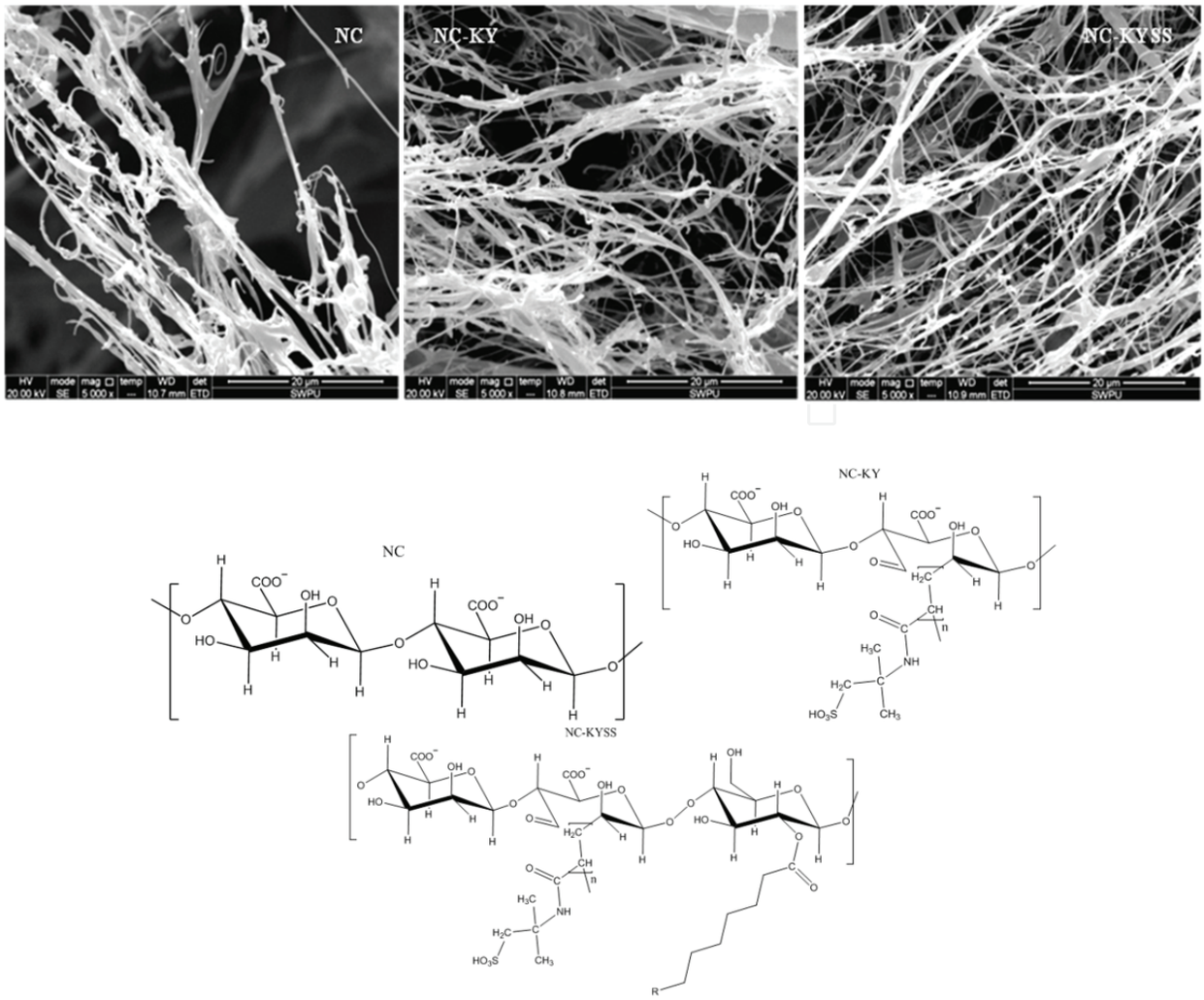

Figure 1. Chemical structure and SEM images of the nanocellulose.

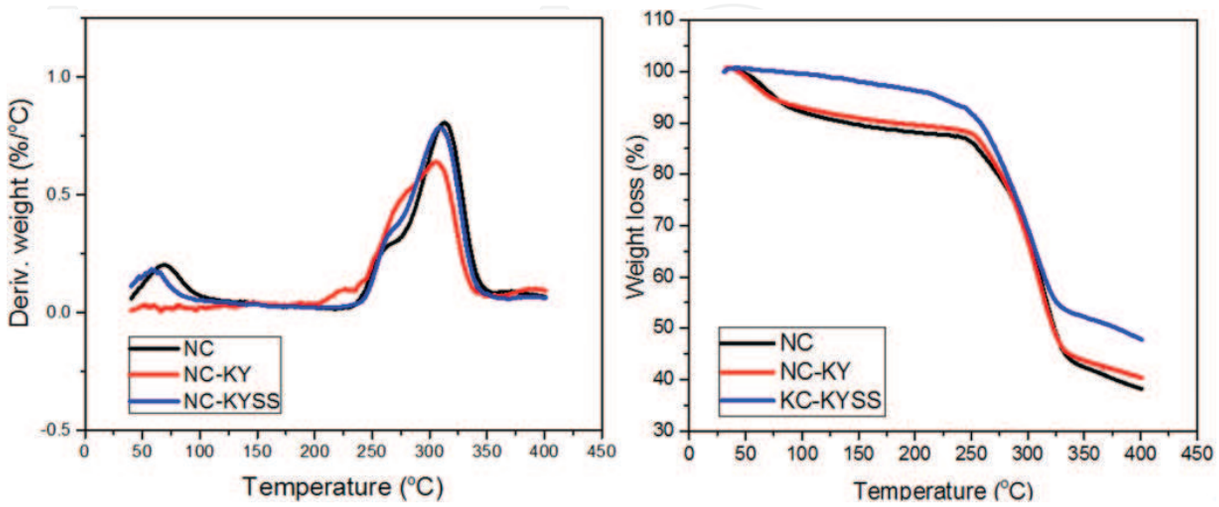

Figure 2. TG/DTG curves of the nanocellulose.

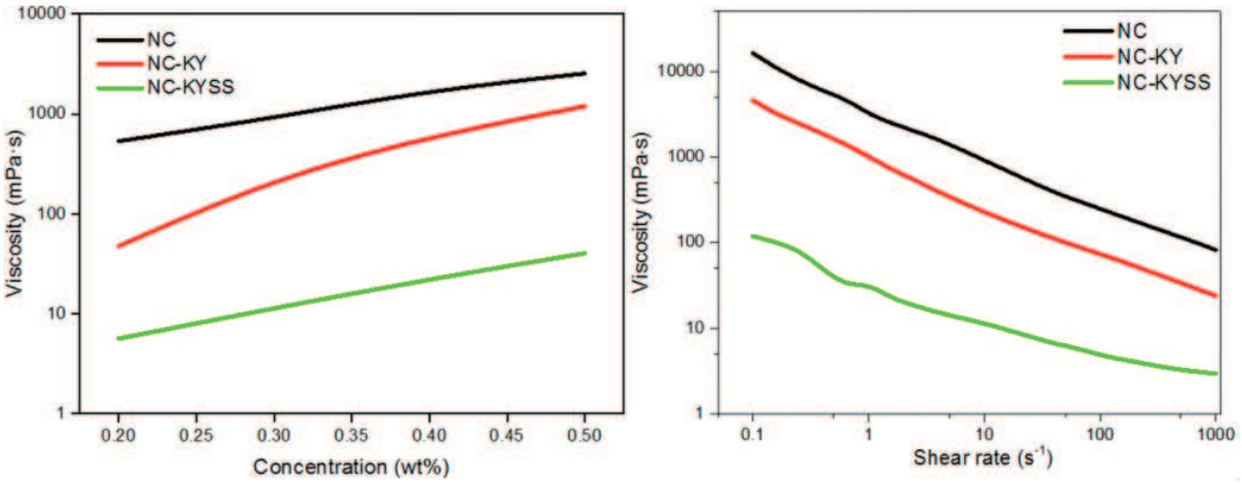

Figure 3. Rheological properties of the nanocellulose fluids.

Figure 4. Images of the nanocellulose nanofluids in electrolyte.

flocculate, subsequently impacting the fluidity in porous media. **Figure 4** presents the images of the nanocellulose fluids in NaCl electrolyte with storage time. It was observed that the ungrafted nanocellulose (NC) fluid remained homogeneous for 30 days in deionized water; however, when the cation was present, nanocellulose aggregation and flocculation occurred as a result of the compressed electric double layer. The grafting of AMPS did not effectively hinder the aggregation. This fact indicated that the sole electrostatic repulsion was not sufficient to combat high salinity. In contrast, simultaneous grafting of AMPS and alkyl chains noticeably enhanced the dispersity of the nanocellulose in electrolyte caused by extra steric hindrance [17].

http://dx.doi.org/10.5772/intechopen.71816

1.4. Microscale displacement behaviors

To study the flow behaviors in porous media and EOR efficiency of the tested nanofluids, a five-spot visual micromodel was designed and assembled in our lab. In addition to visual observation, the propagations of the displacing phase and displaced phase were captured and further analyzed using a coded MatLab program. Due to the dispersity issue, NC-KYSS fluid was first tested in the oil displacement experiment. In the homogenous sand pack model, the waterflooding oil recovery was nearly 46% of original oil in place (OOIP) at 4 PV of brine. Then, a 0.4 PV of NC-KYSS fluid slug was injected into the model to simulate EOR followed by a post waterflooding. It was shown that this nanofluid was able to further improve the oil recovery after waterflooding. In our work, approximately 6% OOIP was produced, and the water cut was reduced simultaneously, verifying the potential of this nanofluid in EOR. **Figure 5** shows the micromodel images captured during the displacement tests. From these images, the reduction of the oil saturation of the sand pack model can be visually observed. Through pixel reading, the oil recovery efficiencies of the waterflooding, nanofluid flooding, and post waterflooding were quantitatively determined as shown in **Figure 6**.

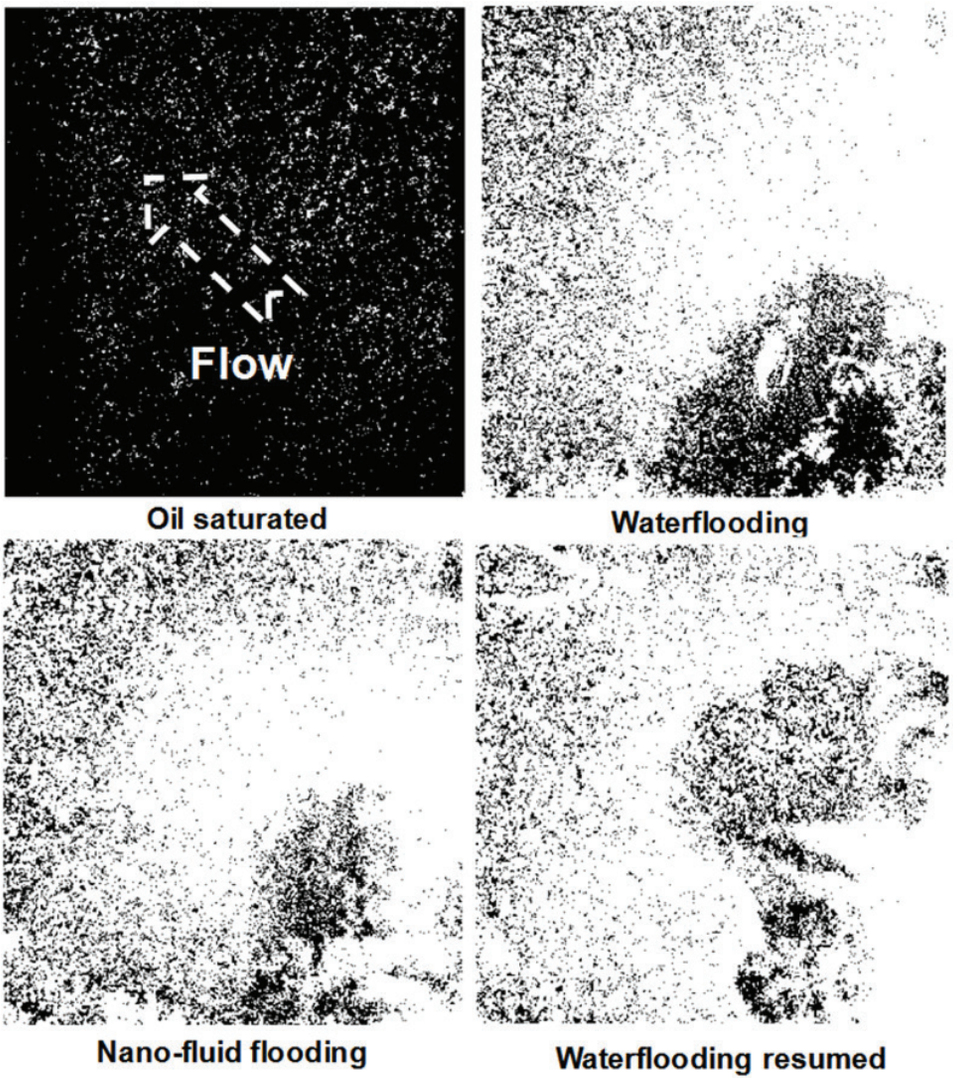

Figure 5. MatLab-released images of the microdisplacement test.

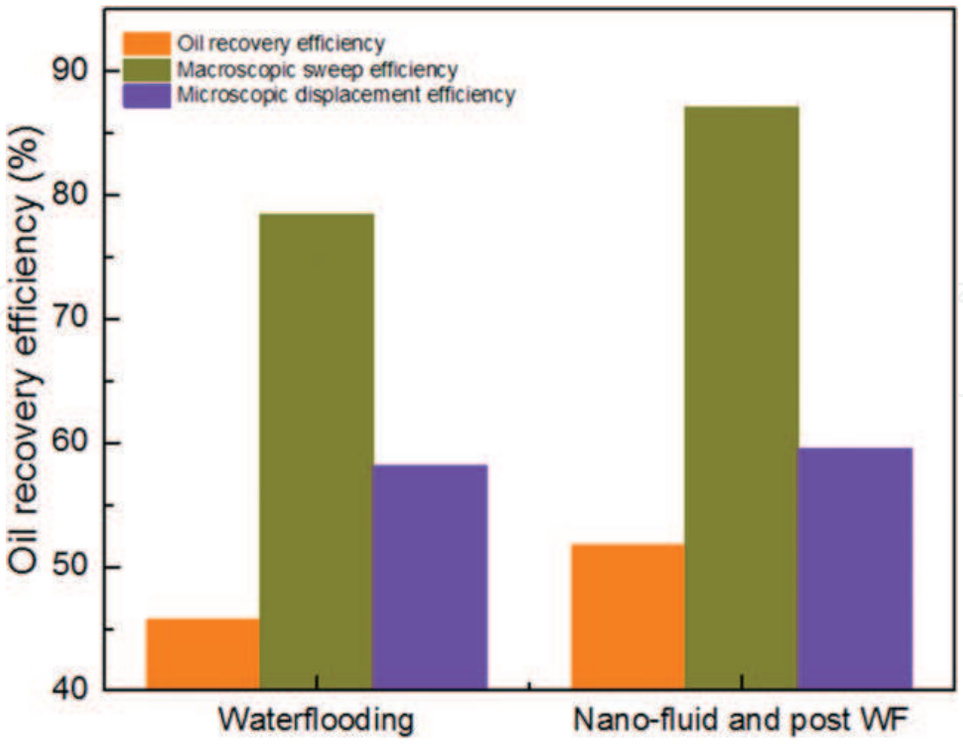

Figure 6. Oil recoveries in the stages of waterflooding and nanofluid flooding.

The results proved that the macroscopic sweep and microscopic displacement efficiencies of the nanofluid flooding were increased by 9.2 and 1.3%, respectively, on the basis of waterflooding [22].

2. Stabilized foam flooding

The EOR efficiency of a foam injection is largely governed by foam stability. However, due to the complex reservoir conditions (pressure, temperature, geological properties, crude, etc.), the generated bubbles in porous media easily rupture particularly when they are in direct contact with hydrocarbons, which are considered as antifoaming agents and detrimental to foam stability [24, 25]. Substantial efforts have been made toward foam stability enhancement from both theoretical and experimental levels [26]. The methods that utilize chemical agents to prevent film drainage have been successfully proposed. The widely used agents can be categorized into two groups, i.e., polymer and nanoparticle. Sydansk observed that adding polymer to the aqueous phase resulted in the improvement of the foam viscosity and stability. Shen et al. compared the stability of HPAM- and xanthan gum-enhanced foam system during migrating in porous media [26]. An associative polymer was also employed to stabilize foam lamella through the molecular interactions with surfactants [27]. Using starch particle to improve the physical properties of foam was suggested by Zhang et al. The results indicated that the film drainage was considerably mitigated owing to starch participation [28]. As for nanoparticle, silica is the most widely used nanoparticle according to reports [29, 30]. Farhadi et al. examined the stability and mobility control of a silica-stabilized CO_2 foam system. It was proved that this system produced uniform and small foams with high apparent viscosity compared to the surfactant-only system

[31]. Hydrophobic silica was also adopted to stabilize a conventional foam system, and the resultant foam system was more rough than that of PEG-coated nanosilica-stabilized foam [32]. In addition to silica, the possibility of aluminum, fly ash, and $CaCO_3$ as foam stabilizers was also assessed [33–35]. Based on the previous works, three possible mechanisms for foam film stabilization were elucidated by Horozov, including monolayer of bridging particles, bilayer of close-packed particles, and network of particle aggregates [36].

2.1. Xanthan gum-stabilized foam

2.1.1. Alteration of foam morphology

As shown in **Figure 7**, CHSB foam displays small and uniform bubble sizes, whereas polymer-enhanced foam presents the large and coarse sizes in the initial state. Afterward, a significant difference is also observed after 10 min, i.e., the bubbles of CHSB foam change into a form of large and polyhedral shape. By contrast, the change behavior of polymer-enhanced foam is very small. Due to the large viscous force, the polymer-surfactant mixtures can create thick and stable liquid films delaying coalescence, which thus promotes the stability of polymer-enhanced foam [37, 38].

2.1.2. Foam microstructure in oil-bearing

In this section, the effect of crude oil on foam properties was shown in **Figure 8**. As observed from **Figure 8(a)**, two systems maintained the favorable foam properties in the presence of 15% oil; nevertheless, the foam stability gradually decreased as the oil content continued to increase. In contrast, the foam volume of the xanthan-enhanced

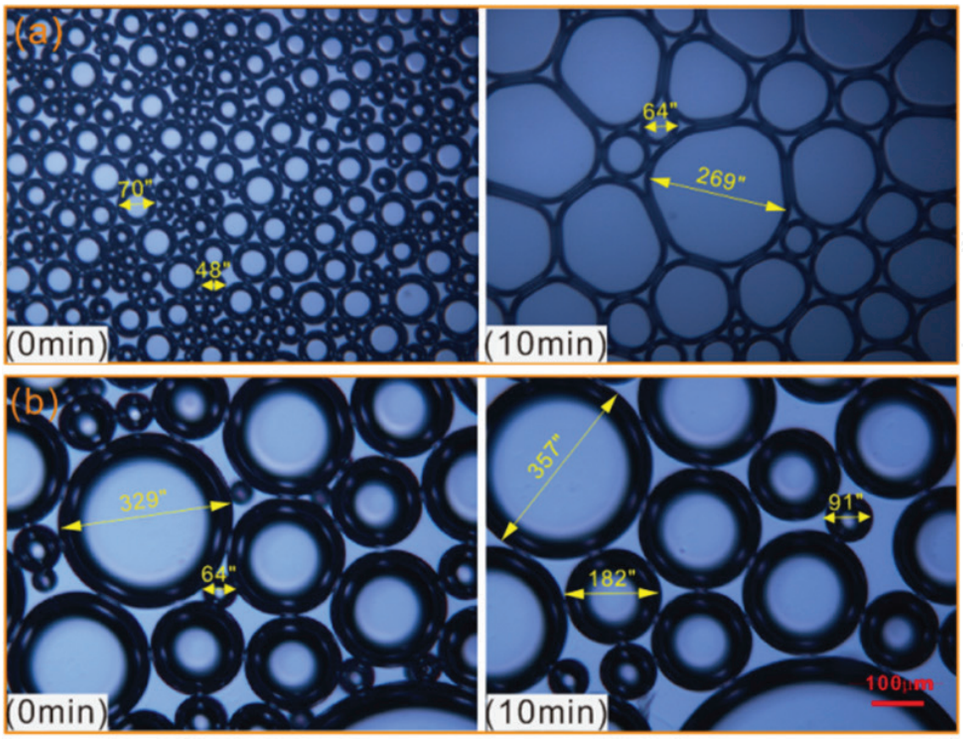

Figure 7. Microstructures of CHSB foam (a) and xanthan-enhanced foam (b) changes over time.

foam increased even when 20% of oil was present, indicating the stabilizing effect of polymer in oil-bearing environment. As shown in **Figure 8(b)**, the half-life ratio was close to 8 in the absence of oil. When the oil was added to the foam system, this ratio nearly remained unchanged within 10% of oil content and then gradually increased to about 10 with the increase of oil content to 20%.

To further evaluate the effect of crude oil on foam, the microstructures of oil foam were visually observed using LM. As shown in **Figure 9(a)**, the oil droplets tended to self-assemble at the plateau borders of CHSB foam with liquid drainage, and the deposited oil droplets merged into the larger drops at a fast rate before finally forming an oil band at the plateau border. From **Figure 9(b)**, the oil droplets of the xanthan-enhanced foam had a smaller size

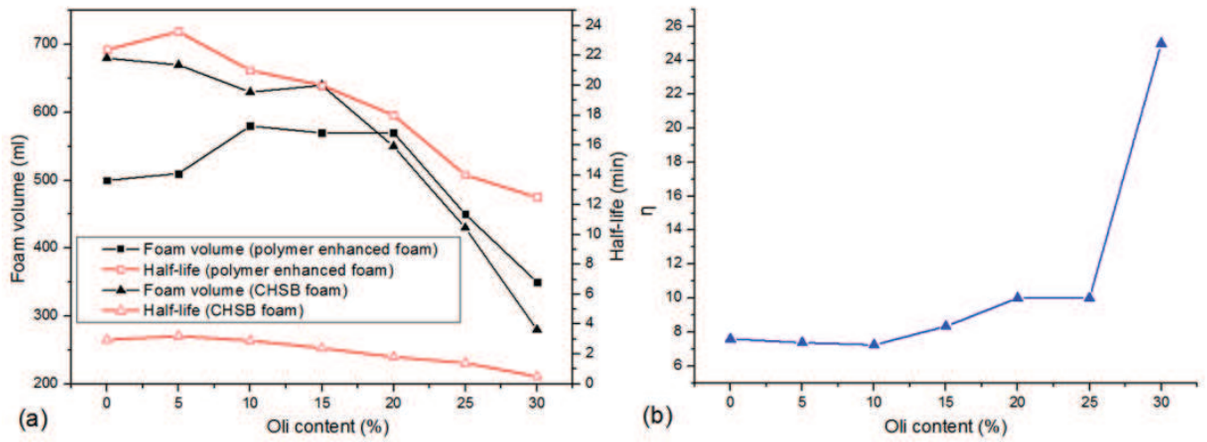

Figure 8. Foam properties as a function of oil content, (a) variations of foam volume and half-time, (b) the half-life ratio (η) of xanthan-enhanced foam to CHSB foam.

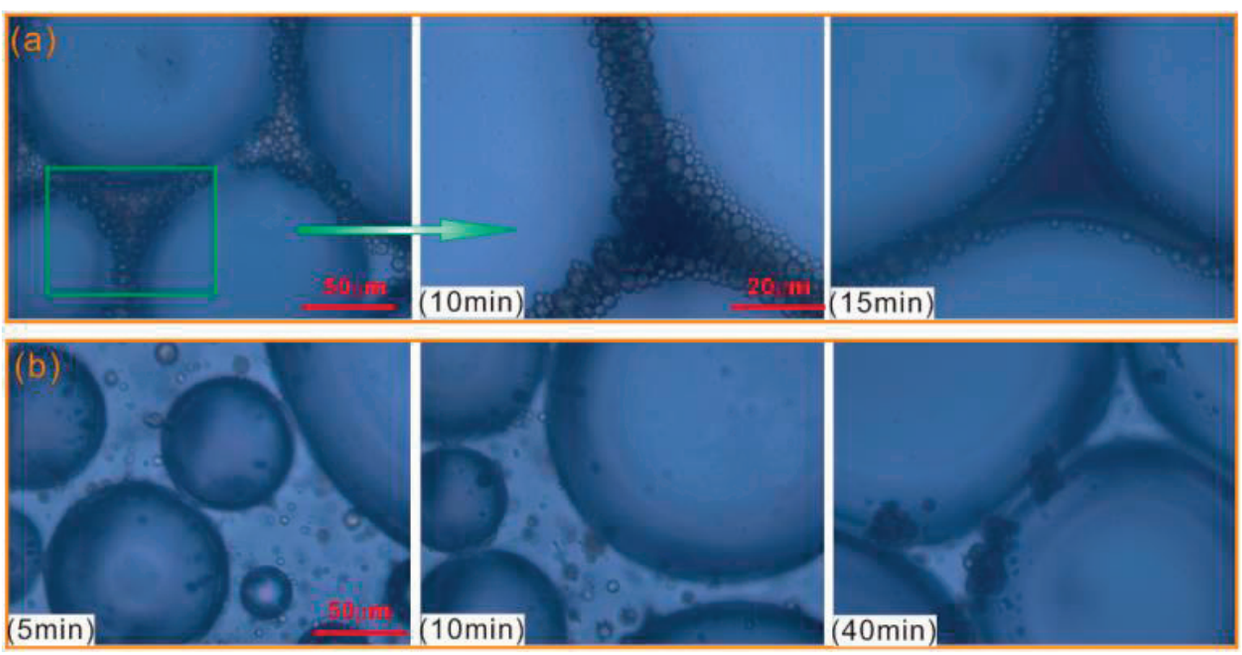

Figure 9. Microphotographs of oil drops as a function of time and CHSB foam (a) and xanthan-enhanced foam (b).

and were uniformly dispersed in the matrix of foam films (i.e., oil in water emulsions). Furthermore, the accumulated oil droplets distributed in foam films instead of plateau borders. As a result, the crude oil can be emulsified into small and stable particles in the foam films.

2.1.3. Foam injection in the heterogeneous model

As shown in **Figure 10**, the oil recovery of high-permeable core is 30–42% after waterflooding, but with the increase of permeability ratio, the oil recovery of low-permeable core decreased, which indicated that the swept volume of the low permeability core was quite low. The remarkable variations of division ratio and oil recovery were observed in heterogeneous cores as a result of the injection of the xanthan-enhanced foam. Since foam gradually established the high flow resistance in the high-permeable core, the subsequent flow was diverted to the low-permeable core displacing the residual oil. Moreover, foam has been proven to perform excellent in the area of low oil saturation and large spatial scale. Therefore, the large amount of crude oil was produced from both the high-permeable core and the low-permeable core, which thus led to the facts that the enhanced oil recovery increased as the heterogeneity gets stronger especially in the low-permeable core.

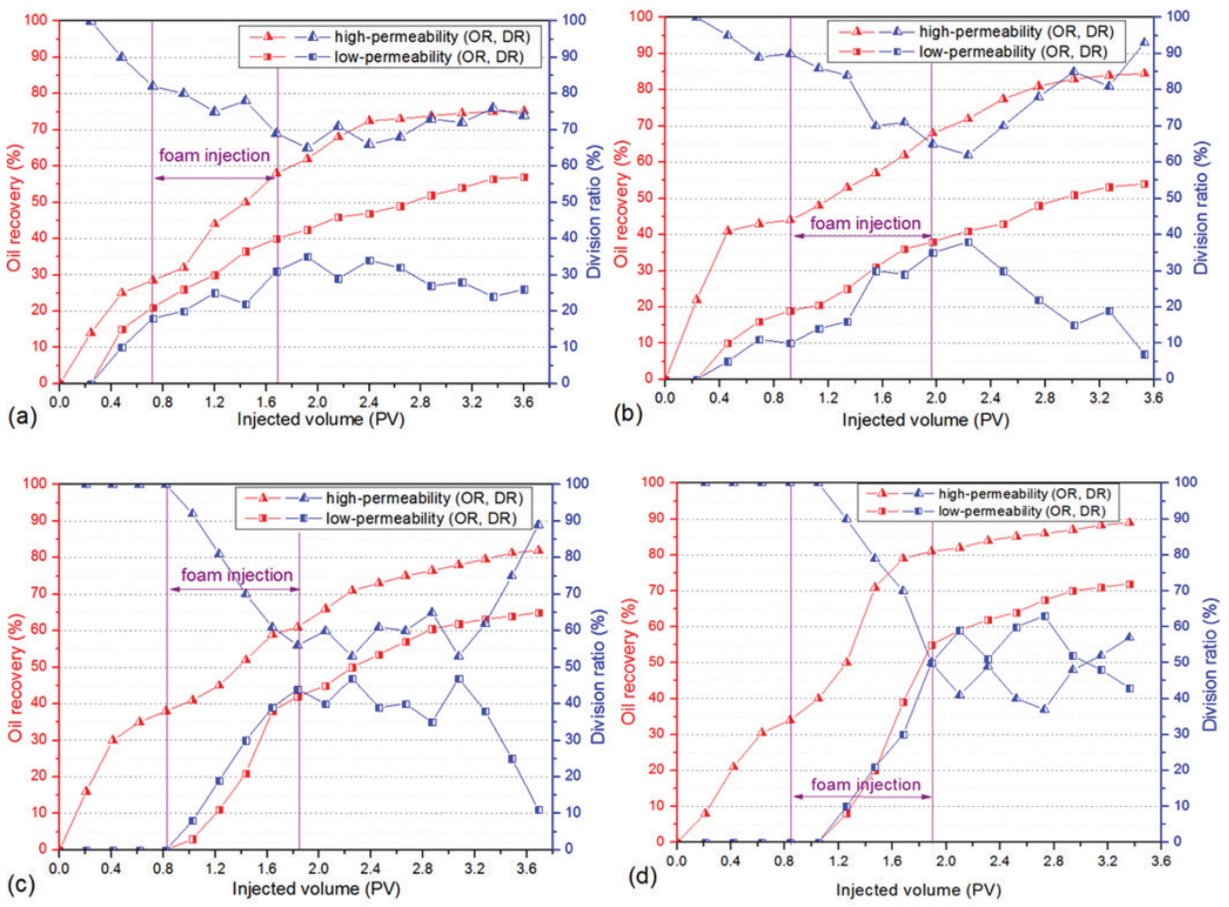

Figure 10. Changes of oil recovery (OR) and division ratio (DR) in the high and low permeability of heterogeneous cores. The different permeability ratios are 1.5 (a), 3 (b), 6 (c), and 12 (d), and xanthan-enhanced foam is injected.

Consequently, the significant flow diversion and oil increase were achieved by conducting polymer-enhanced foam flooding in the heterogeneous formation. The larger permeability ratio can promote the advantage of foam to carry out mobility reduction and oil recovery enhancement.

2.2. Nanocellulose-stabilized foam

2.2.1. Foam decay in the absence and presence of crude oil

Figure 11 shows the foam decay profiles of the four systems in the absence and presence of oil. In the bulk tests, the criterion of half decay time, which was defined as the time that the first half foam volume lasts, was frequently used to quantify the stability of the prepared foam. Normally, long half decay time represents high foam stability and vice versa. The incorporation of the nanocellulose fluids notably extended the foam life from generation to completely vanish. The enhancement was more significant when oil was present, as revealed by the profiles shown in the right. These profiles also demonstrated that oil was detrimental to foam stability. After nanofluid stabilization, the half decay time or stability of the foam was considerably promoted. The hypothesized mechanisms of foam lamella stabilization are as follows. Due to the synergism of the nanocellulose molecules, the close-packed foam lamella is further strengthened, which consequently renders the generated bubbles less probability to rupture. Moreover, the substantial OH- groups on the nanocellulose surface are also capable of impeding liquid drainage owing to the hydrogen bonding interactions between water, nanocellulose, and surfactant molecules in the film lamella. The close-packed foam lamella leads the foam volume to shrink due to the increased liquid viscosity and density, whereas the molecular interactions at the foam lamella can stabilize the foam film and accordingly extend the foam life [22].

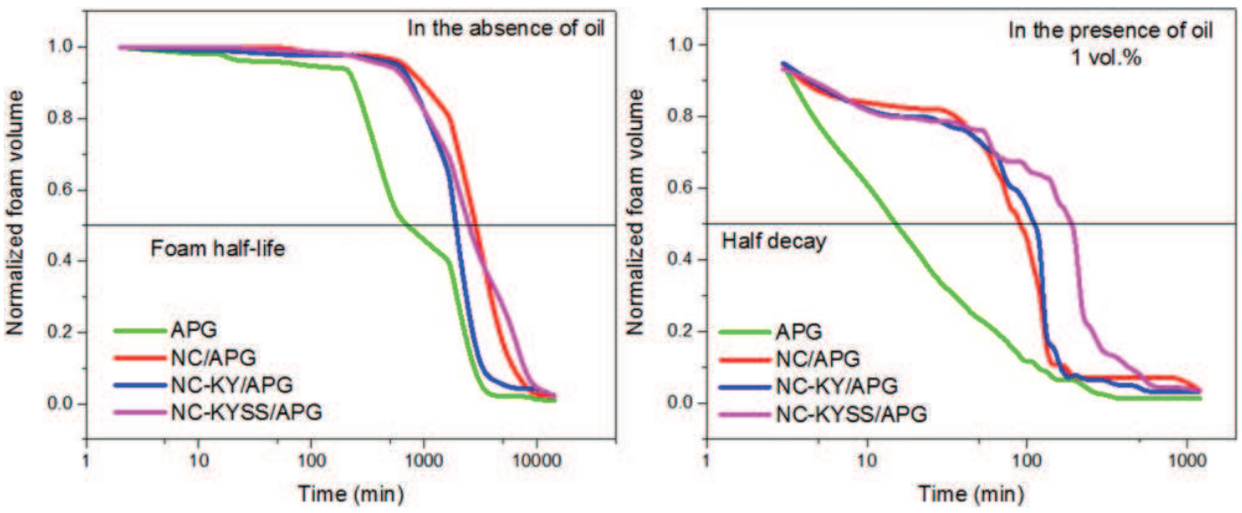

Figure 11. Foam decay profiles of four systems (APG: foaming agent).

http://dx.doi.org/10.5772/intechopen.71816

2.2.2. Morphology of the stabilized foam

The participation of NC-KYSS made the resultant bubbles smaller than the surfactant-only foam, which subsequently led to thicker foam lamella due to the stabilizing effect as shown in **Figure 12**. This effect enables the prepared foam to retard inter-bubble gas diffusion. When hydrocarbons were present, the improvement of the foam lamella thickness was more significant. The microscopic observations were highly in agreement with the results obtained in the bulk cylinder tests. The coarsening rate of the foam bubbles was accelerated when hydrocarbons were involved and consequently resulted in large bubbles. Although the hydrocarbons have exerted a detriment to foam morphology, considerably thick foam lamella was constructed due to the collaboration of NC-KYSS. The reasons behind to interpret this fact have been discussed above [22].

2.2.3. Microdisplacement behaviors

Using the same digital method as established in Section 1.4, the flow patterns of oil and foam in porous media were captured as shown in **Figure 13**. The residual oil saturation (S_{or}) represented by the black pixel indicated the limited oil recovery of waterflooding stage. As foam injection proceeded, an "oil bank" was constructed in the front of foam as a result of the mobilized residual oil. However, due to the defoaming/antifoaming effect, the conventional foam quickly channeled/fingered through the established oil bank leaving oil-bearing area untouched. In contrast, the injection of the KYSS-stabilized foam created a tough and "piston-like" displacing front owing to the prominent oil tolerance and accordingly promoted the macroscopic sweep efficiency and microscopic displacement efficiency as shown in **Figure 14** [22].

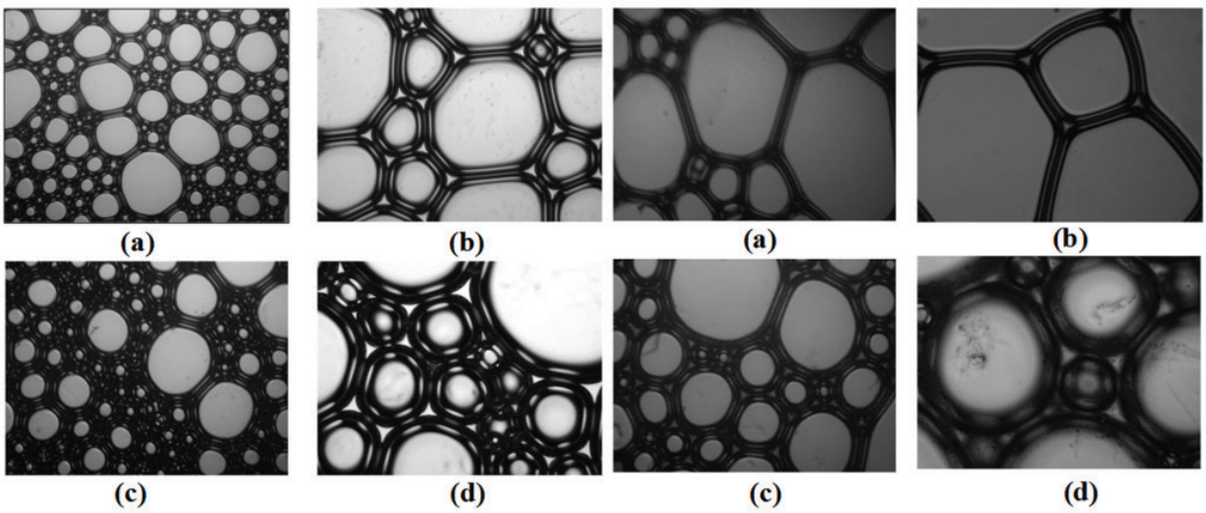

Figure 12. Microscopy images of the foam (a and b: APG foam at 40 and 100×; c and d NC-KYSS-stabilized foam at 40 and 100×).

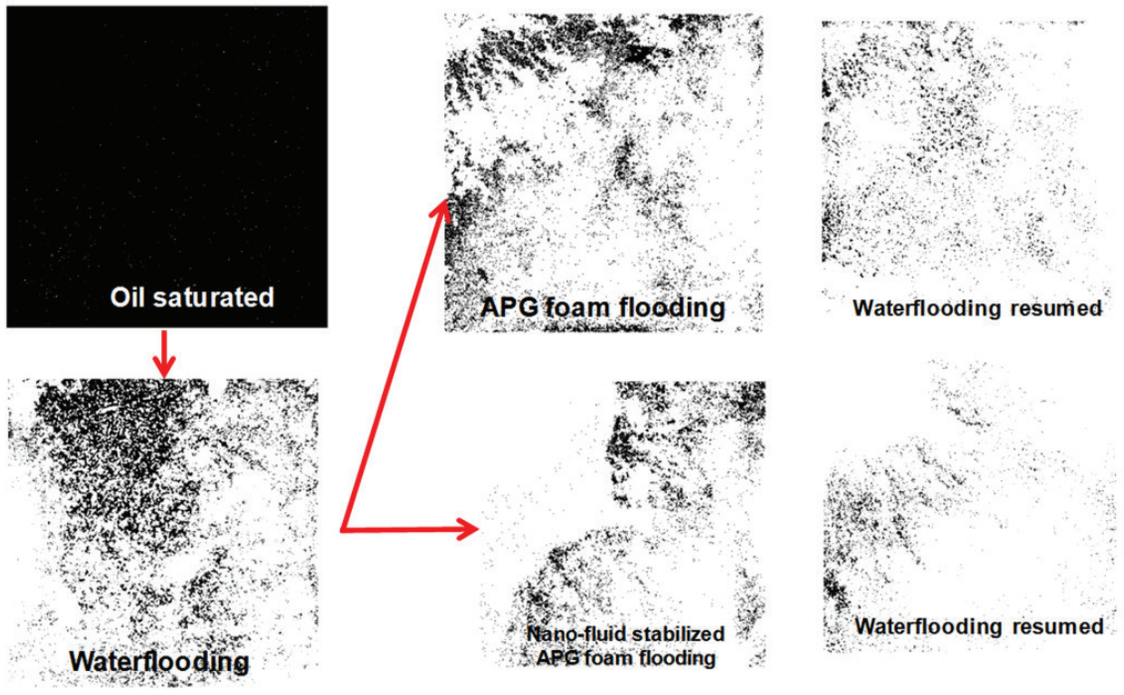

Figure 13. MatLab-released images of the foam flooding.

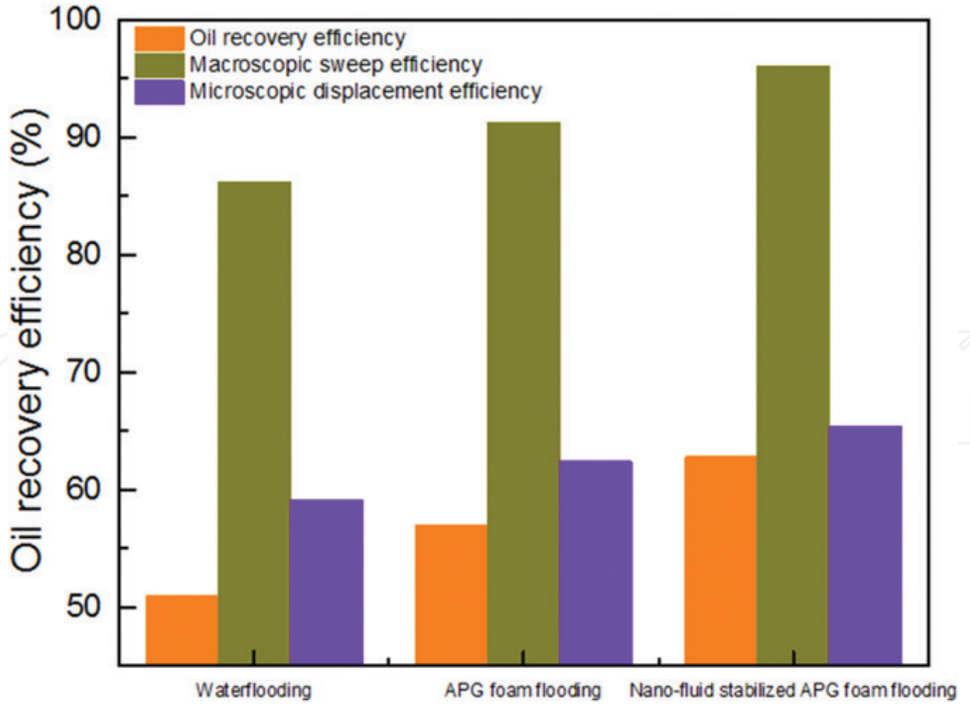

Figure 14. Oil recovery efficiencies of the foam flooding.

http://dx.doi.org/10.5772/intechopen.71816

3. Microsphere injection

After extensive waterflooding, most of the oilfields worldwide have entered the middle and high water cut stage; crude oil production decreases significantly. Meanwhile, the exploration of new oil and gas resources is becoming more and more difficult. In order to maintain the oil production of the aged oilfield, to find an economical and effective enhanced oil recovery (EOR) technique has become the focus of researchers.

In the last decade, a new dispersion gel called polymer microspheres (PMs) was employed for high temperature and salinity reservoirs to achieve conformance control. The PMs that match well with pore-throat size can be synthesized via the polymerization of polymer monomer, crosslinking agent, initiator, and active agent. The associated physical properties and dynamic displacement behaviors of PMs synthesized by inverse emulsion polymerization in our laboratory would be discussed briefly in next sections aiming at rendering quite a few evidences guiding its application in actual reservoirs.

3.1. Physical properties of PMs

As shown in **Figure 15**, the PMs were micron-grade particles with milky white and high sphericity. The initial particle size distribution of PMs synthesized by inverse emulsion polymerization in our laboratory was in the range of 2.364 (d_{10}) to 26.212 μm (d_{90}), and its median diameter (d_{50}) was 9.996 μm (see **Figure 16**) [39].

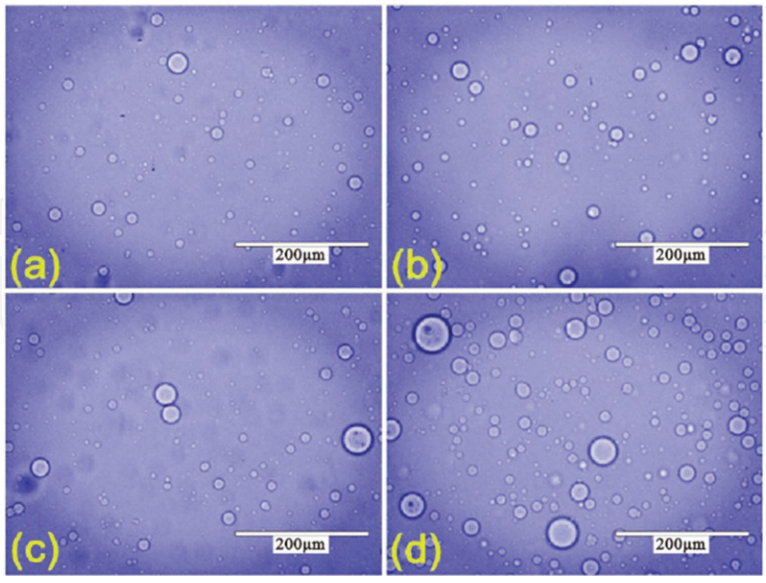

Figure 15. Dispersion state of PM system at different times: (a) initial state, (b) 10 minutes, (c) 20 minutes, and (d) 30 minutes.

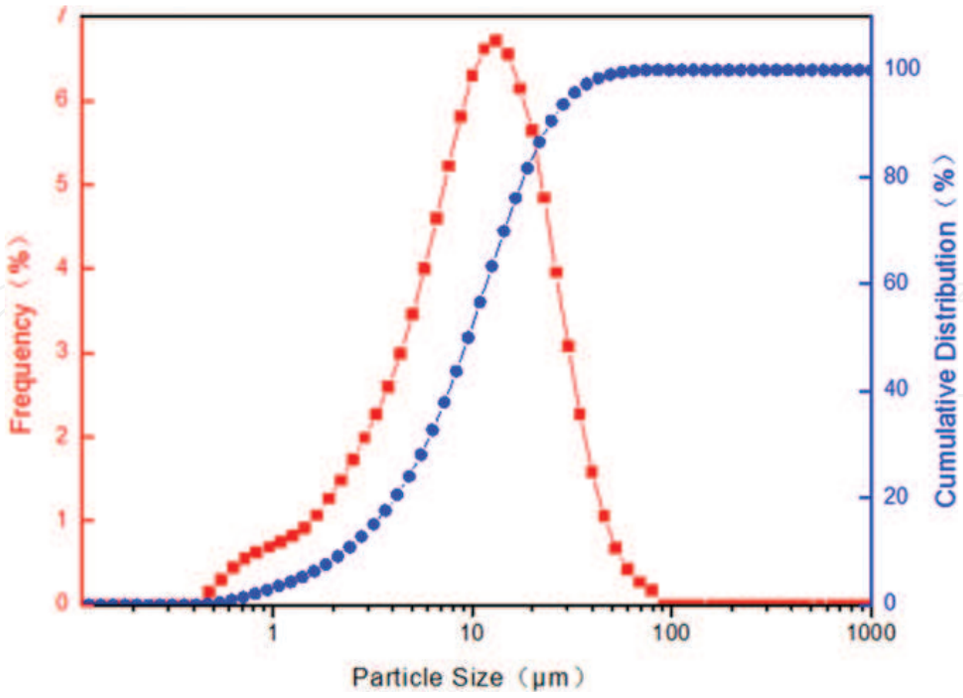

Figure 16. Initial particle size distribution of PMs in the injection water.

Figure 15(a)–(d) shows the morphology of PMs swelling for 15 days in injection water at 25, 50, 75, and 104°C, respectively. The PMs kept high sphericity and could well disperse in water with no precipitation and agglomeration within the temperature ranging from 25 to 104°C. The results show that the PMs could withstand temperature of 104°C and salinity of 25,000 mg/L. This renders PMs' potential in high temperature and salinity reservoirs.

The hydration swelling property of PMs is represented by the expansion ratio, which can be calculated by Eq. (1):

$$ER = (D_2 - D_1)/D_1 \quad (1)$$

where ER represents expansion ratio and D_1 and D_2 are median diameter of PMs before and after expansion, respectively, μm.

The changing curves of the expansion ratio of PMs under different salinity conditions at 25°C are shown in **Figure 17**. At the same salinity, the expansion ratio of PMs increased with time; the expansion rate in the initial stage was fast, then gradually slowed down, and leveled up after swelling for 7 days. At the same hydration time, the expansion ratio of PMs decreased with the salinity. In particular, the swelling ratio of PMs in the deionized water was much larger than that in the brine.

Figure 18 displays the apparent viscosity of 0.5 wt% PM system in the deionized water, NaCl solution with salinity of 10,000 and 20,000 mg/L, reservoir injection water, respectively, after swelling 10 days at 25°C. In the range of low shear rate, the apparent viscosity of PM system

http://dx.doi.org/10.5772/intechopen.71816

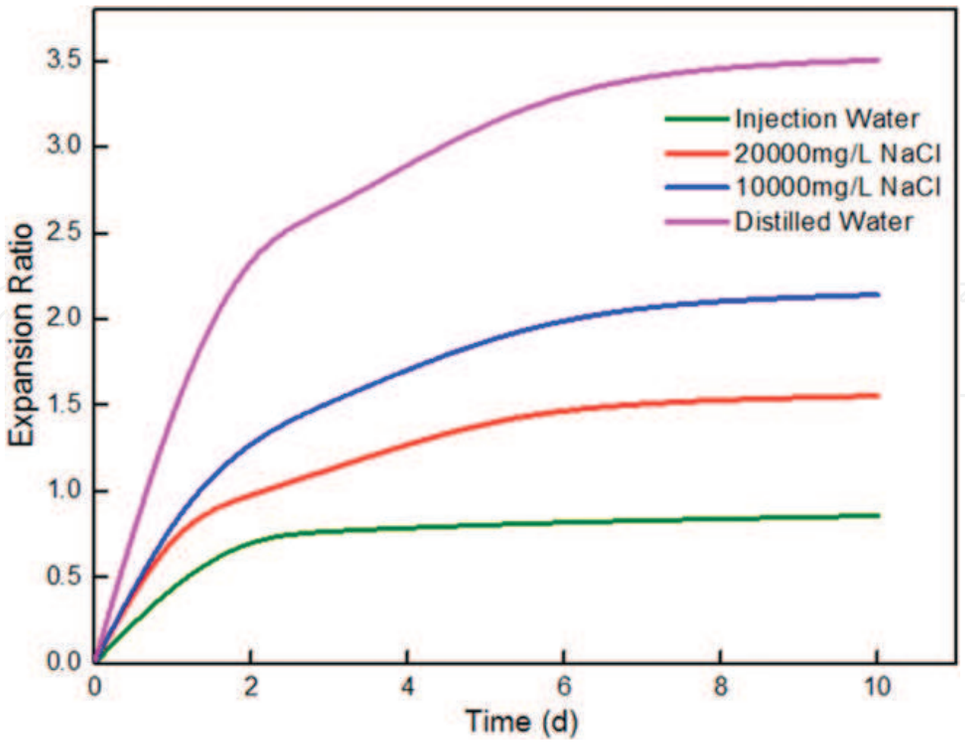

Figure 17. Influence of salinity on the expansion ratio of PMs.

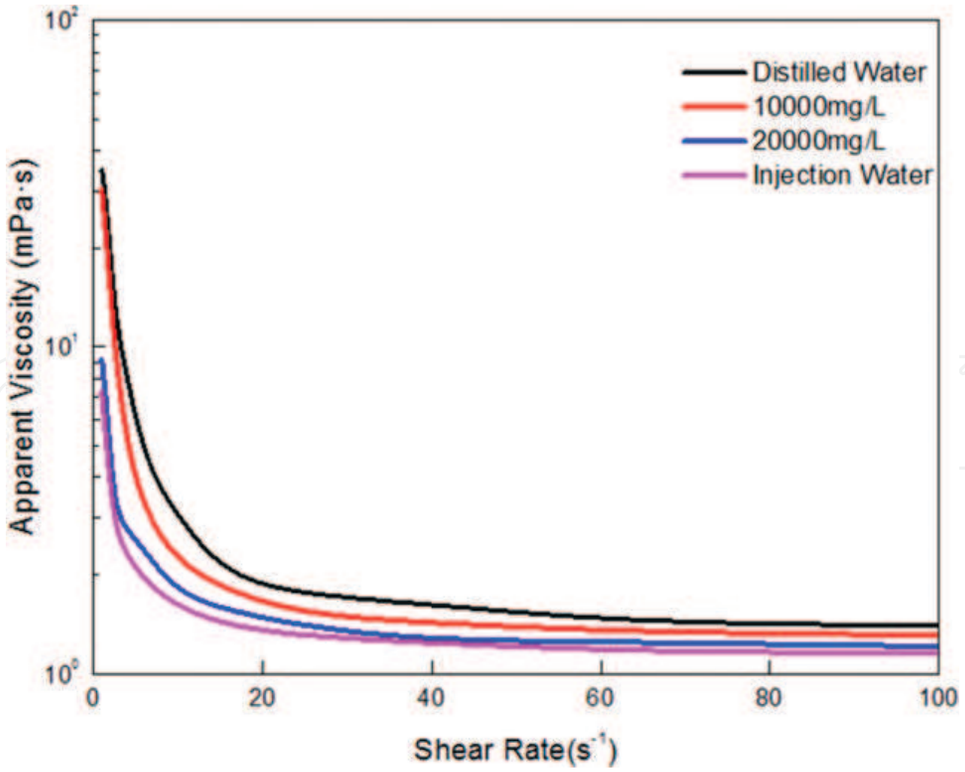

Figure 18. Apparent viscosity of PM system versus the shear rate (25°C).

decreased significantly with the shear rate. At the high shear rate, the apparent viscosity of PM system increased or decreased slightly with the shear rate, which is close to the viscosity of water. So the original water injection pipeline could be directly used to inject the PM system. The dynamic elasticity of four types of PMs (without solvent) mentioned in this section versus frequency is shown in **Figure 19**. For the same PMs, when the oscillation frequency was increased from 0.1 to 100 Hz, the elastic modulus of PMs gradually increased. At the same frequency, the elastic modulus of PMs increased with the salinity, which is related with the charge of PMs [39].

3.2. Dynamic displacement behaviors of PMs

The fluid distribution of the visual model, in which diagonal upper and lower area represents low and high-permeable zone, respectively, is shown in **Figure 20**. During PMF, the PM system mainly flowed into the high-permeable zone. In the SWF stage (**Figure 20(d)**), the low-permeable zone was significantly activated evidencing these PMs can achieve effective plugging for high-permeable region as well as allow the subsequent fluid to flow into the low-permeable zone rich in remaining oil [40].

3.3. Matching relationship between microsphere diameter and pore-throat size

As shown in **Figure 21**, the migration type with $\beta > 1.99$ (the ratio of median diameter of PMs and average pore-throat diameter of core) is defined as "complete plugging," in which the pressure drop increased noticeably with the injection of PM system. "High-efficiency plugging" arises

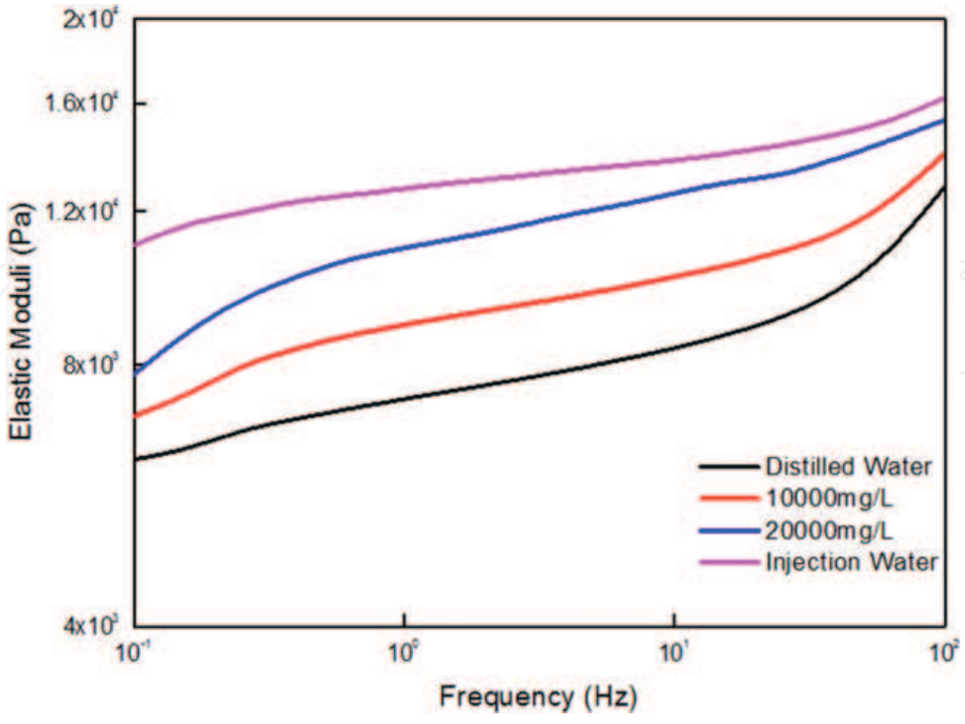

Figure 19. Elastic modulus of PMs versus the frequency (25°C).

http://dx.doi.org/10.5772/intechopen.71816

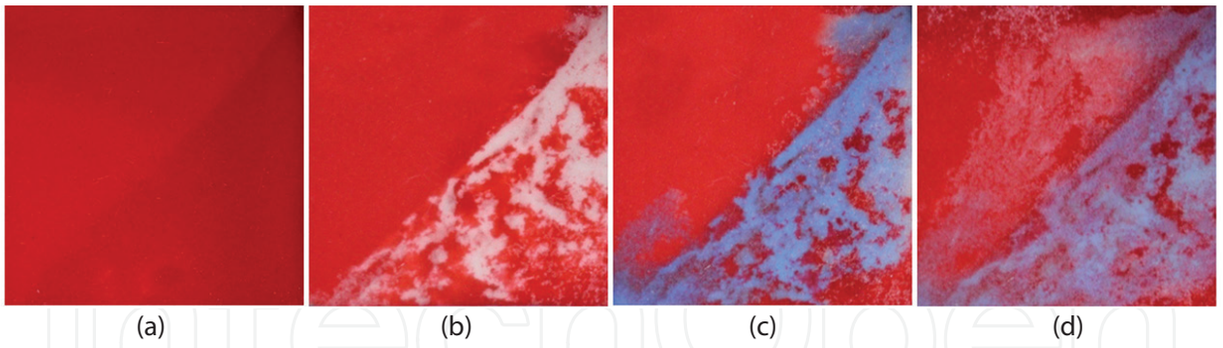

Figure 20. Fluid distribution of the visual model (a) initial oil saturation, (b) WF, (c) PMF, and (d) SWF.

when β is in the range of 1.02 and 1.99. In this case, the differential pressure first increased with the injection of PMs until a peak pressure was achieved. This demonstrated the plugging of the pore throats. Afterward, the pressure curve tended to fluctuate with the injection continued, indicating that the PMs might break up and thus pass through the pore throats and then deeply migrate forward into the core until the next block-breakthrough cycle occurred. The differential pressure gradually decreased before finally leveling off during SWF. The resistance coefficient and blocking rate were more than 21.9 and 80.9%, respectively. In the case of $0.59 < \beta < 1.02$, the migration was regarded as "low-efficiency plugging," in which the differential pressure varied similarly with "high-efficiency plugging" with exception of the causing lower pressure. The relevant resistance coefficient and blocking rate were 8.3–21.9 and 20–80.9%, respectively. "Smooth pass" occurred when β is smaller than 0.59. The blocking rate was less than 20% including the reduction of cross-sectional area caused by the adsorption of PMs on the pore surfaces. Hence, the majority of the PMs passed the pore throats successfully without any plugging effect [39].

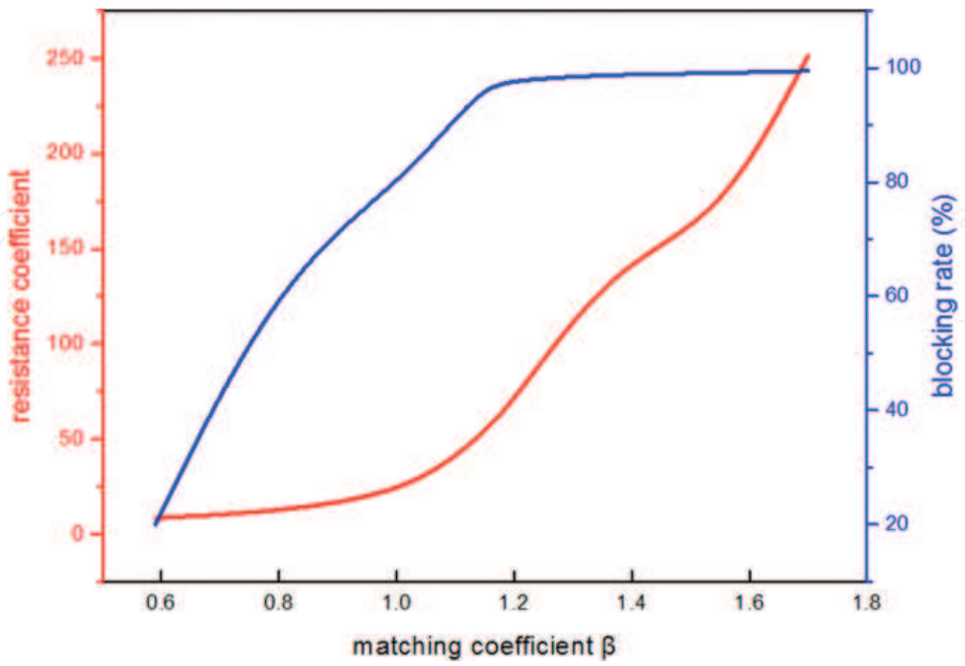

Figure 21. Resistance coefficient and blocking rate versus matching coefficient.

Acknowledgements

The authors gratefully acknowledge the financial support provided by the Canadian Foundation for Innovation (CFI), National Key Basic Research Program of China (2015CB250904), and PetroChina Innovation Foundation (2015D-5006-0212).

Author details

Bing Wei*, Peng Wei, Shuai Zhao and Wanfen Pu

*Address all correspondence to: bwei@swpu.edu.cn

State Key Laboratory of Oil and Gas Reservoir Geology and Exploitation, Southwest Petroleum University, Chengdu, China

References

[1] Wei B, Romero-Zerón L, Rodrigue D. Evaluation of two new self-assembly polymeric systems for enhanced heavy oil recovery. Industrial and Engineering Chemistry Research. 2014;**53**(43):16600-16611

[2] Kusanagi K, Murata S, Goi Y, Sabi M, Zinno K, Kato Y, Togashi N, Matsuoka T, Liang Y. Application of cellulose nanofiber as environment-friendly polymer for oil development. In: Paper SPE 176456 presented at SPE/IATMI Asia Pacific Oil & Gas Conference and Exhibition

[3] El Ela MA, Sayyouh H. An integrated approach for the application of the enhanced oil recovery projects. Journal of Petroleum Science and Engineering. 2014;**3**:176-188

[4] Cheraghian G, Hendraningrat L. A review on applications of nanotechnology in the enhanced oil recovery part A: effects of nanoparticles on interfacial tension. International Nano Letters. 2016;**1**:1-10

[5] Wilson A. Molecular-dynamics study examines effect of nanoparticles on oil/water flow. Journal of Petroleum Technology. 2013;**65**(02):148-151

[6] Yang X, Liu ZH. A kind of nanofluid consisting of surface-functionalized nanoparticles. Nanoscale Research Letters. 2010;**5**(8):1324-1328

[7] Kwak K, Kim C. Viscosity and thermal conductivity of copper oxide nanofluid dispersed in ethylene glycol. Korea-Australia Rheology Journal. 2005;**17**(2):35-40

[8] Khairul M, Shah K, Doroodchi E, Azizian R, Moghtaderi B. Effects of surfactant on stability and thermo-physical properties of metal oxide nanofluids. International Journal of Heat and Mass Transfer. 2016;**98**:778-787

[9] Hendraningrat L, Li S, Torsæter O. A coreflood investigation of nanofluid enhanced oil recovery. Journal of Petroleum Science and Engineering. 2013;**111**:128-138

[10] Buckley JS, Fan T. Crude oil/brine interfacial tensions. Petrophysics. 2007;**48**(03):175-185

[11] Hendraningrat L, Torsæter O. A stabilizer that enhances the oil recovery process using silica-based nanofluids. Transport Porous Media. 2015;**108**(3):679-696

[12] Roustaei A, Saffarzadeh S, Mohammadi M. An evaluation of modified silica nanoparticles' efficiency in enhancing oil recovery of light and intermediate oil reservoirs. Egyptian Journal of Petroleum. 2013;**22**(3):427-433

[13] Onyekonwu MO, Ogolo NA. Investigating the use of nanoparticles in enhancing oil recovery. SPE Paper 140744 Present at Nigeria Annual International Conference and Exhibition. Society of Petroleum Engineers. 2010

[14] Ehtesabi H, Ahadian MM, Taghikhani V. Enhanced heavy oil recovery using TiO_2 nanoparticles: Investigation of deposition during transport in Core plug. Energy & Fuels. 2014;**29**(1):1-8

[15] Lv YZ, Wang J, Yi K, Wang W, Li C. Effect of oleic acid surface modification on dispersion stability and breakdown strength of vegetable oil-based Fe_3O_4 nanofluids. Integrated Ferroelectrics. 2015;**163**(1):21-28

[16] Wei B, Li Q, Jin F, Li H, Wang C. The potential of a novel nano-fluid in enhancing oil recovery. Energy & Fuels. 2016;**30**(4):2882-2891

[17] Li Q, Wei B, Xue Y, Wen Y, Li J. Improving the physical properties of nano-cellulose through chemical grafting for potential use in enhancing oil recovery. Journal of Bioresources and Bioproducts. 2016;**4**(1):186-191

[18] Eichhorn SJ, Dufresne A, Aranguren M, Marcovich NE, Capadona JR, Rowan SJ, Weder C, Thielemans W, Roman M, Renneckar S. Review: Current international research into cellulose nanofibres and nanocomposites. Journal of Materials Science. 2010;**45**(1):1-33

[19] Sathvika T, Manasi M, Rajesh V, Rajesh N. Microwave assisted immobilization of yeast in cellulose biopolymer as a green adsorbent for the sequestration of chromium. Chemical Engineering Journal 2015;**279**:38-46

[20] Janardhnan S, Sain MM. Isolation of cellulose microfibrils-an enzymatic approach. BioResources. 2006;**1**(2):176-188

[21] Klemm D, Schumann D, Kramer F, He08ler N, Hornung M, Schmauder HP, Marsch S. Nanocelluloses as innovative polymers in research and application. Advances in Polymer Science. 2006;**205**:49-96

[22] Wei B, Li H, Li Q, Wen Y, Sun L, Wei P, Pu WF, Li YB. Stabilization of foam lamella using novel surface-grafted nanocellulose-based nanofluids. Langmuir. 2017;**33**(21):5127-5139

[23] Li QZ, Wei B, Lu LM, Li YB, Wen YB, Pu WF, Li H, Wang CY. Investigation of physical properties and displacement mechanisms of surface-grafted nano-cellulose fluids for enhanced oil recovery. Fuel. 2017;**207**(13):352-364

[24] Nikolov AD, Wasan DT, Huang DW, Edwards DA. The effect of oil on foam stability: Mechanisms and implications for oil displacement by foam in porous media. Paper SPE 15443 Presented at SPE Annual Technical Conference and Exhibition. Society of Petroleum Engineers. 1986

[25] Xu X, Saeedi A, Liu K. Laboratory studies on CO_2 foam flooding enhanced by a novel amphiphilic ter-polymer. Journal of Petroleum Science and Engineering. 2015;**138**:153-159

[26] Shen C, Nguyen QP, Huh C, Rossen WR. Does polymer stabilize foam in porous media? Paper SPE 99796 Presented at SPE/DOE Symposium on Improved Oil Recovery. Society of Petroleum Engineers. 2006

[27] Hernando L, Bertin H, Omari A, Dupuis G, Zaitoun A. Polymer-enhanced foams for water profile control. Paper SPE 179581 Presented at SPE Improved Oil Recovery Conference. Society of Petroleum Engineers. 2016

[28] Zhang YQ, Chang ZD, Luo WL, Gu SN, Li WJ, An JB. Effect of starch particles on foam stability and dilational viscoelasticity of aqueous-foam. Chinese Journal of Chemical Engineering 2015;**23**(1):276-280

[29] Khajehpour M, Etminan SR, Wassmuth F, Bryant S. Nanoparticles as foam stabilizer for steam-foam process. Paper SPE 179826 Presented at SPE EOR Conference at Oil and Gas. 2016

[30] Emrani AS, Nasr-El-Din HA. Stabilizing CO_2-foam using nanoparticles. Paper SPE 174254 Presented at SPE European Formation Damage Conference and Exhibition. 2013

[31] Farhadi H, Riahi S, Ayatollahi S, Ahmadi H. Experimental study of nanoparticle-surfactant-stabilized CO_2 foam: Stability and mobility control. Chemical Engineering Research & Design. 2016;**111**:449-460

[32] Worthen A, Chen Y, Bryant S, Bagaria H, Huh C, Johnston K. Nanoparticle stabilized carbon dioxide in water foams for enhanced oil recovery. Paper SPE 154285 Presented at SPE Improved Oil Recovery Symposium. Society of Petroleum Engineers. 2012

[33] Zhou Y, Li Y, Yuan J. The stability of aluminum foams at accumulation and condensation stages in gas injection foaming process. Colloids and Surfaces, A: Physicochemical and Engineering Aspects. 2015;**482**:468-476

[34] Eftekhari AA, Krastev R, Farajzadeh R. Foam stabilized by fly-ash nanoparticles for enhancing oil recovery. Industrial and Engineering Chemistry Research. 2015;**54**(50):12482-12491

[35] Cui ZG, Cui YZ, Cui CF, Chen Z, Binks BP. Aqueous foams stabilized by in situ surface activation of $CaCO_3$ nanoparticles via adsorption of anionic surfactant. Langmuir. 2010;**26**(15):12567-12574

[36] Horozov TS. Foams and foam films stabilised by solid particles. Current Opinion in Colloid & Interface Science. 2008;**13**(3):134-140

[37] Pu WF, Wei P, Sun L. Stability, CO 2 sensitivity, oil tolerance and displacement efficiency of polymer enhanced foam. RSC Advances. 2017;**7**(11):6251-6258

[38] Pu WF, Wei P, Sun L. Experimental investigation of viscoelastic polymers for stabilizing foam. Journal of Industrial and Engineering Chemistry. 2017;**47**:360-367

[39] Zhao S, Pu WF, Wei B, Xu XG, A comprehensive investigation of polymer microspheres (PMs) migration in porous media: EOR implication. Submitted to Fuel

[40] Pu WF, Zhao S, Wei B. Research on the profile control and displacement mechanisms of polymer microspheres. Submitted to Energy Fuels

IntechOpen